Supporting Information

Ultrathin Mesoporous F-doped α-$Ni(OH)_2$ Nanosheets as an Efficient Electrode material for Water Splitting and Supercapacitor

Nadeem Hussain[1], Wenjuan Yang, [5,6],Jianmin Dou,[2] Yanan Che[4,], Yitai Qian[1] and Liqiang Xu[1,3*]*

[1]Key Laboratory of Colloid & Interface Chemistry, Ministry of Education and School of Chemistry and Chemical Engineering, Shandong University, Jinan, 250100, China.

[2] School of Chemistry and Chemical Engineering, Liaocheng University, Liaocheng, 252000, China

[3] Key Laboratory of Advanced Energy Materials Chemistry (Ministry of Education), Nankai University, Tianjin 300071, China

[4] School of Materials Science and Engineering, Tianjin University, Tianjin, 300350, China

[5] Department of Chemistry, Tsinghua University, Beijing 100084, China.

[6] School of Chemistry and Chemical Engineering, Yulin University, Yulin City 719000, Shaanxi, China.

Email: xulq@sdu.edu.cn; yananchen@tsinghua.edu.cn

Experimental Section

Synthesis of F-doped α-$Ni(OH)_2$

The mesoporous F-doped α-$Ni(OH)_2$ nanosheets were prepared by using one-step solvothermal process without any surfactant or hard templates. In a typical process, 0.234 g trisodium citrate dehydrated was added into the mixed solvents of ethylene glycol and water (36+1 ml) and stirrer few minutes then added 0.5139 g $NiCl_2.6H_2O$ and stirrer another several minutes until a clear solution formed, and then sodium acetate trihydrated (1.08 g) was added with continuous stirring and finally different amount of ammonium fluoride (0.8 g, 0.16 g, 0.24 g and 0.32 g) was added and stirrer for another one hour and then transferred to Teflon autoclave and heated for 12 h at 200ºC. After the autoclave was cooled to room temperature naturally, green color product was finally obtained after the centrifugation and post-treatment process (washed with distilled water and ethanol several times and then dried at 60ºC overnight). Simple α-$Ni(OH)_2$ without F intercalation was prepared by using urea instead of ammonium fluoride.

Synthesis of β-$Ni(OH)_2$

β-$Ni(OH)_2$ was prepared using the same method but pH value was adjusted to 11using NaOH instead of CH_3COONa.

Characterization

The structure of the obtained material was determined by powder XRD system equipped with graphite-monochromatized Cu Kα radiation ((λ = 1.5418 Å). The structure of material was tested by field emission scanning electron microscopy (FESEM, ZEISS SUPRA 55), transmission electron microscopy (TEM, JEM-1011) and high resolution transmission electron microscopy

(HRTEM, JEOL-JEM-2100F). A Fourier transformation infrared (FTIR) spectrum was recorded on a ALPHA-T system with KBr pellets (4000−400 cm-1). XPS tests were performed on a Kratos AXIS Ultra DLD spectrometer using an Al Ka X-ray source. Thermogravimetric analysis (TGA, TA Q500) was performed in air with a heating rate of 10ºC/min in the temperature range of 10-700ºC. Brunauer–Emmett–Teller (BET) surface area and nitrogen adsorption isotherm were measured over P/P_o = 0-1 at 77 K on an autosorb IQ (Quantachrome, USA). The thickness of sheets was analyzed by a cipher ES (Asylum Research) AFM in tapping mode, whose cantilever was OMCL-AC160TS-R3 (Olympus) having a nominal spring constant of 26 N/m and nominal resonant frequency of 300 kHz by using SiO_2 sheet as a substrate. Gas chromatography measurements were conducted on Techcomp 7890 || GC equipped with a 5 Å molecular sieve column with N_2 as the carrier gas and thermal conductivity detector (TCD).

Electrochemical Measurements

OER measurements

To measure the electrochemical performance of the obtained material, rotating disk electrode experiments were performed in a three electrode electrochemical cell with potentiostate. 10 mg of the sample was added into 5ml water-isopropyl alcohol mixture (3:2) with 20 µl Nafion solution and one hour ultrasonicated for homogeneous mixture. 20 µl ink (40 µg catalyst) was loaded on polished glassy carbon electrode (5mm diameter) and dried overnight. All the tests were performed in 1 M KOH solution (pH = 13.6), using Hg/HgO as a reference electrode, and O_2 passed for 0.5h before testing. Before all electrochemical measurements, cyclic voltammetry (CV) is carried out at 50mV scan rate for several cycles at rotating disk with 1600 rpm for activation of catalyst. Linear sweep voltammetry were studied at 10 mV s^{-1} scan rate between voltage windows of 1.175 to 1.85

V (vs RHE). Tafel slop was derived from LSV. The electrochemical impedance spectroscopy (EIS) was recorded between 0.1Hz to 1 MHz at 400 mV overpotential. The Nyquist plot was obtained from EIS data.

TOF value was calculated by following equation at η=350mv:

$$\text{TOF} = \frac{jS}{4 \times F \times n}$$

Where J is measured current at specific overpotential, 4 is a number of electron per mole of O_2, F is a faraday's constant (96485.3 ºC mol^{-1}) and n is the number of moles of the metal, calculated from given mass of metal and molecular mass of a compound. Chronoamperometry measurement was used to test long time stability by loading catalyst 5 mg on Ni foil (1x1cm^2) at overpotential of 320 mV. The Faradaic efficiency was calculated by comparing the amount of measured oxygen with calculated oxygen at 1.7 V (vs RHE). The amount of evolved oxygen was quantified using a Techcomp 7890 || GC equipped with a 5 Å molecular sieve column with N_2 as the carrier gas and thermal conductivity detector (TCD). Figure S1 shows the protocol for measuring electrocatalytic properties of studied Catalysts for OER.[1]

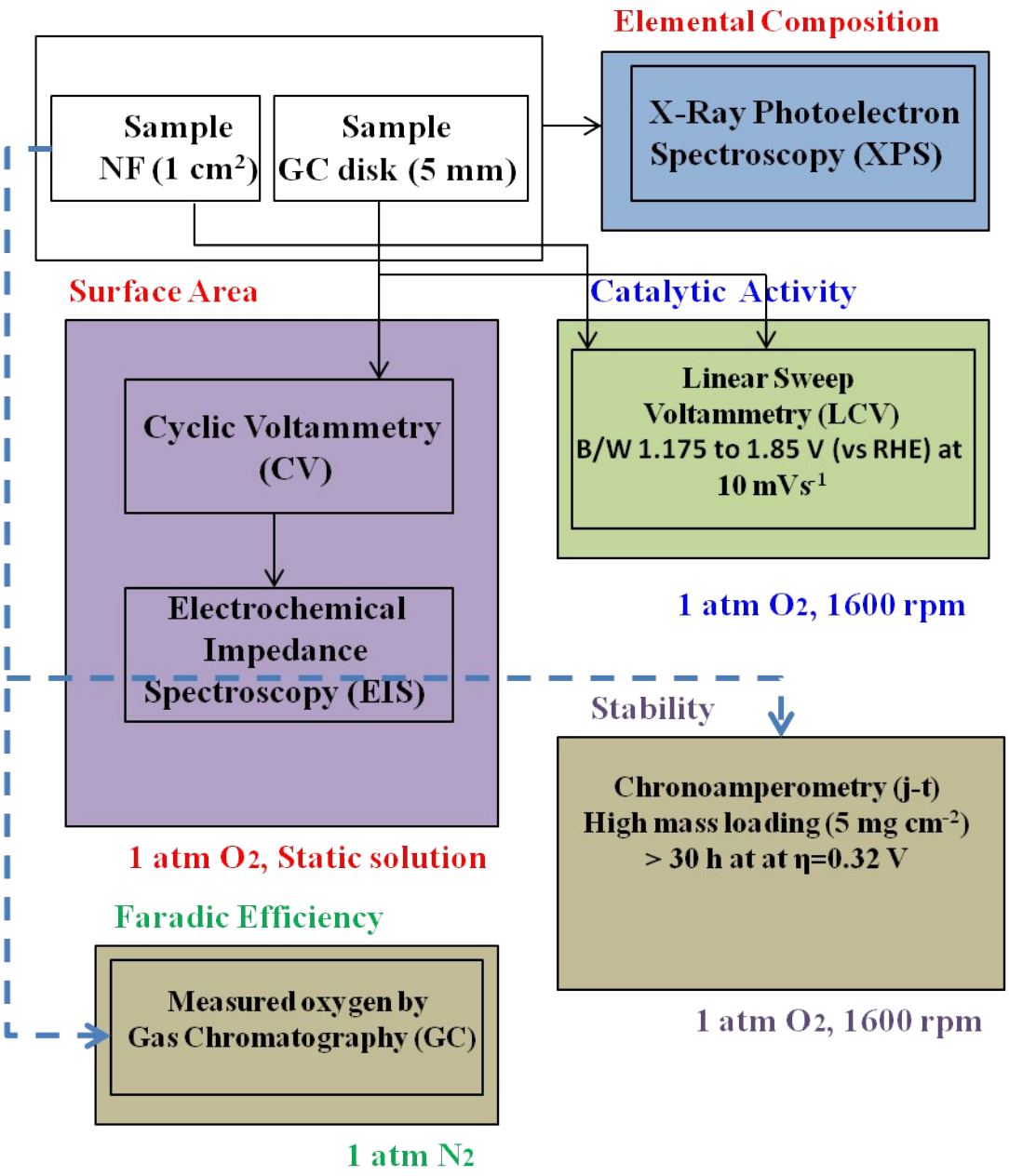

Figure S 1. Protocol for measuring electrocatalytic properties of studied Catalysts for OER.

Supercapacitor measurements

The working electrode was prepared by mixing 80% active material, 14% carbon black and 6% PTFE binder. The slurry was dropped on clean Ni foil (1x1 cm^2) and dried at 60ºC for 12 hours. 2

M aqueous solution of KOH was used as electrolyte. Cyclic voltammetry (CV), galvanometric charge-discharge (GCD) and electrochemical impedance spectroscopy (EIS) measurements were evaluated in a conventional three electrode cell at room temperature by using CHI760E electrochemical work station. Before testing, working electrode was put in 2 M KOH solution for 12 h for activation. The loading mass of active material was 2-3 mg. For long cyclic stability LAND CT2001A battery test system was used.

The specific capacitance was calculated from galvanostatic charging-discharging (GCD) curve by using the following equation:

$$C = \frac{I\Delta t}{m\Delta V}$$

Where C (F g^{-1}) is specific capacitance, I (A g^{-1}) is current density, Δt (s) discharging time, m (g) loaded weight of active material and ΔV is the voltage window during discharging.

Fabrication of Asymmetric device

Activated carbon (AC) used as negative electrode and F intercalated α-$Ni(OH)_2$ as a positive electrode. Both of the electrodes were prepared using the same procedure mentioned above for preparation of individual electrode. NKK, TF4840 separator with 2 M KOH electrolyte was used for the fabrication of ASC. Mass balance equation was used to calculate the mass ratio between cathode and anode.

$$\frac{m^-}{m^+} = \frac{C_+ \times V_+}{C_- \times V_-}$$

$$\frac{m^-}{m^+} = \frac{1503 \times 0.53}{200 \times 1}$$

$\frac{m^-}{m^+} \approx 4$

Energy density and power density were calculated by the following equations:

$$E = \frac{1}{2}CV^2$$

$$P = \frac{E}{\Delta t}$$

Where, E (W h kg^{-1}) is energy density, C (F g^{-1}) is specific capacitance, V is voltage window, P (W kg^{-1}) is power density and Δt (sec) is discharging time.

Computational method

Our calculations were based on the density functional theory (DFT) with the Perdew–Burke–Ernzerhof version[2] of the generalized gradient approximation (GGA-PBE) for the exchange–correlation potential, as implemented in a plane-wave basis code VASP.[3, 4] The pseudo-potential was described by the projector-augmented-wave (PAW) method.[5] The geometry optimization is performed until the Hellmann–Feynman force on each atom is smaller than 0.01 eV $Å^{-1}$ during the atomic structure optimization. The atoms were optimized with a conjugate gradient (CG) method.[6] The numerical integration in the first Brillouin zone is performed using a Monkhorst–Pack grid of 7 × 7 × 1 for the surface. We optimized NiOOH with lattice constants a =2.819 Å, b = 2.44 Å and c = 20.65Å, in good agreement with the experimental value of a = 2.819, b = 2.44 Å and c = 20.65 Å.

The adsorption energies were calculated according to the equation, Eads = E(adsorbate/substrate) - [E(substrate) + E(adsorbate)], where E(adsorbate/substrate), E(substrate) and E(adsorbate) represent the total energy of substrate with adsorbed species, the clean substrate and the molecule in the gas phase, respectively. Each electrochemical reaction step of methanol oxidation involves a (H+ + e-) pair transfer from the adsorbed species on the surface to the electrolyte. The free energy change of each (H+ + e-) pair transfer reaction was calculated using the computational hydrogen electrode (CHE) method developed by Nørskov et al.[7, 8] At standard condition (U = 0, pH = 0, p = 1 bar, T =298 K), the free energy ΔG0 of the reaction *AH → A + H+ + e-, can be calculated as the free energy of the reaction *AH → A + 1/2H2. ΔG0 = ΔE + ΔZPE + Δ0→298KΔH – TΔS, is calculated as follows: The reaction energy ΔE = E(product) - E(reactant). ΔZPE, ΔH and ΔS denote the difference in zero point energy, enthalpy, and entropy due to the reaction, respectively. The enthalpy and entropy of the ideal gas molecule were taken from the standard thermodynamic Tables.[9] Therefore, reaction free energy can be calculated by the equation: ΔG (U, pH, p = 1 bar, T = 298 K) =ΔG0 + ΔGpH + ΔGU, where ΔGpH is the correction of the free energy of H+-ions at a pH different from 0: ΔGpH = -kTln[H+] = kTln10 × pH. ΔGU =-eU, where U is the electrode potential relative to the standard hydrogen electro

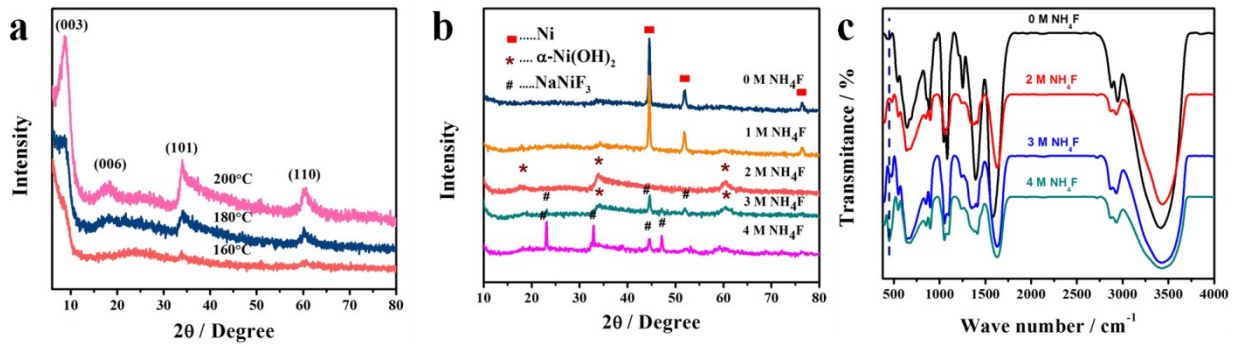

Figure S 2. (a) XRD patterns of F-doped α-$Ni(OH)_2$ prepared at different temperatures. (b) XRD patterns of the obtained samples at different concentrations of NH_4F. (c) FT-IR spectrum of the obtained samples at different concentrations of NH_4F.

The obtained product without ammonium fluoride during synthesis was only composed of solid spheres (Figure S3a). All the diffraction peaks in the XRD pattern (Figure S2b, dark blue line) can be indexed to be Ni metal (PDF#04-850).The addition of ammonium fluoride influences the morphology and crystal nature of product. When the molar ratio of Ni source and ammonium fluoride was the same then no significant change occurred in XRD pattern (orange line, Figure S2b) but in morphology solid spheres Co-existed with sheets (Figure S3b). However, dramatic changes occurred in both morphology and crystal nature if the molar ratio between Ni source and ammonium fluoride was increased. Pure phase of α-$Ni(OH)_2$ mesoporous sheets was obtained when twice molar concentration of ammonium fluoride than Nickel source (red line, Figure S2b) was used, where the F^- was intercalated between the layers, therefore, no extra peaks observed in XRD pattern, but just increase the interlayer distance. When the molar concentration of NH_4F was increased from twice of Ni source then extra peaks observed in XRD pattern (green and purple line, Figure S2b), which indicates the formation of $NaNiF_3$. Similar evidence was obtained from FT-IR spectrum, when the F source concentration was up to twice of Ni source, the spectrum show the formation of α-$Ni(OH)_2$ and there is no evidence of Ni-F bond formation. However, when the molar concentration of NH_4F was increased from twice of Ni source then extra peaks observed in

XRD pattern (green and purple line, Figure S2a), as well as in FT-IR spectrum (dotted line at 449 cm^{-1}, Figure S2b). The sharp peak at 450 cm^{-1} indicated the Ni-F bond formation,[10-12] which was absent when the concentration of F source was twice or less than twice than Ni source.

The corresponding transmission electron microscopy (TEM) images are shown in Figure S3. When different molar ratios of Ni source and NH_4F were used, the material has morphologies of solid spheres (1:0), solid spheres plus sheets (1:1), 2D curly mesoporous sheets (1:2), irregular thick sheets (1:3) and sheets plus irregular nanoflakes (1:4).

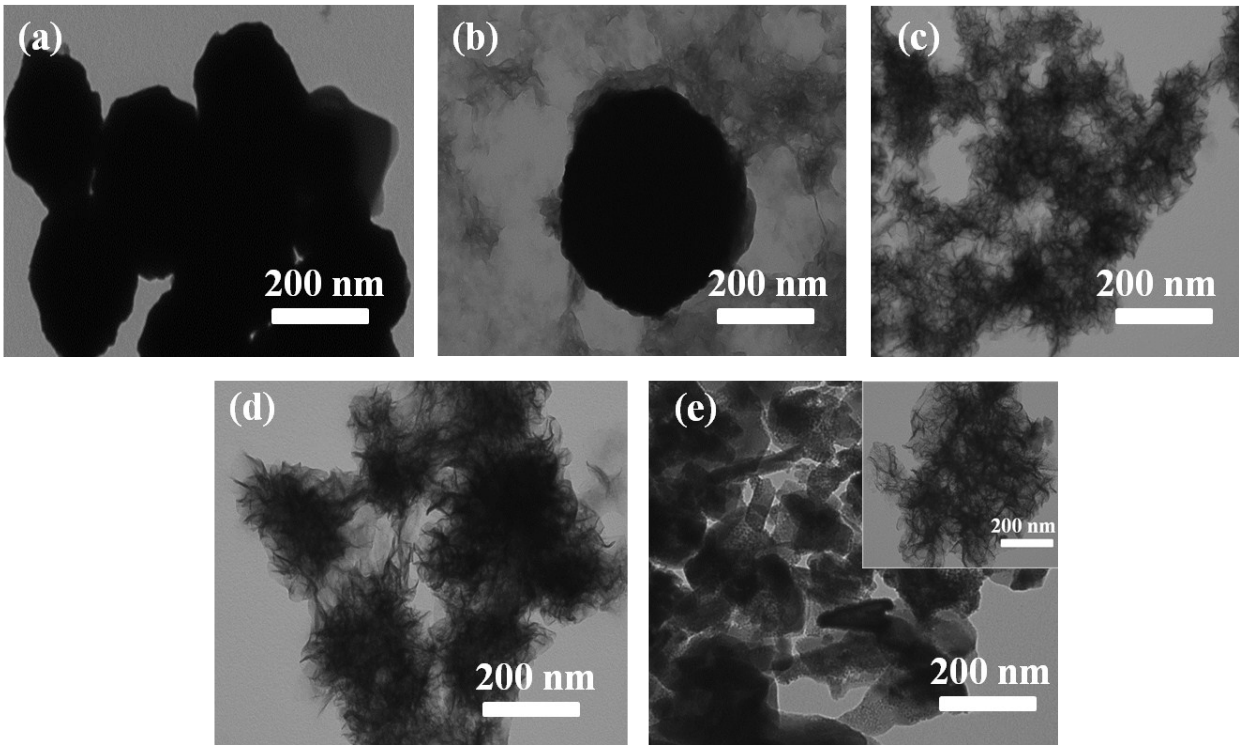

Figure S 3. Effect of NH_4F concentration on the morphology of final product, (a) absence of NH_4F, (b) equal molar ratio between Ni and NH_4F, (c) twice molar ratio of NH_4F than Ni, (d) 3 times molar ratio of NH_4F than Ni, (e) 4 times moles ratio of NH_4F than Ni.

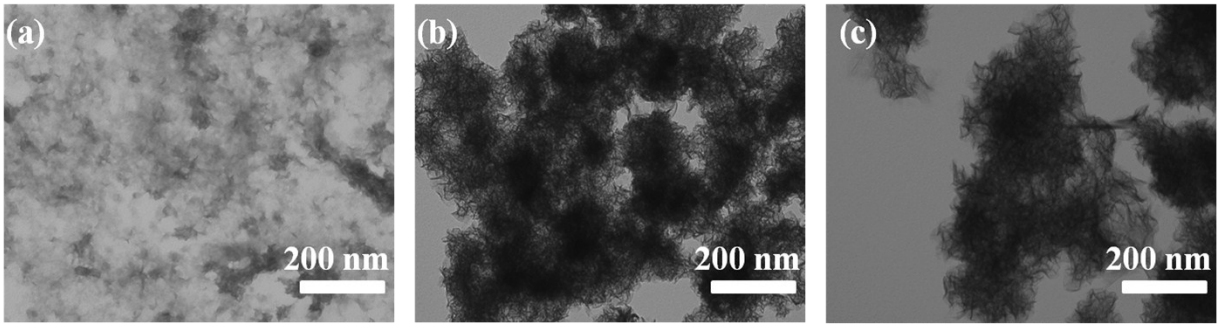

Figure S 4. Effect of temperature at twice concentrations of NH_4F than Ni, (a) 160ºC, (b) 180ºC, (C) 200ºC

The precursor concentration in solvent and the synthesis temperature is critical for the formation of F-doped α-$Ni(OH)_2$ nanosheets with high crystallinity (Figure S2). A series of contrast experiments have been carried out to investigate the effects of solvents and other regents on the final morphology and structure of α-$Ni(OH)_2$. In the absence of sodium acetate (the pH value is ~ 5), only aggregated microscale sheets (Figure S5a) were obtain, and the product is a mixture of α -$Ni(OH)_2$ and $NaNiF_3$ (Figure S5b). For comparison, in the presence of sodium acetate, the pH value of reaction solution was increased to 6.5 at room temperature and further increased after heating due to continued dissociation of sodium acetate and reaction occurred in slightly basic media, where, F-doped α-$Ni(OH)_2$ was formed. In addition, β-$Ni(OH)_2$ was obtained (Figure S9) when reaction was performed in highly basic media (pH ≥11). Hence, we can conclude that the pH is very important factor to obtain the pure phase α-$Ni(OH)_2$ with specific morphology. It is noticeable that solvent is a very important influencing factor on the final structure and morphology of product. To study the effect of solvent on morphology and structure of α-$Ni(OH)_2$, different experiments were performed at various ratios of solvents (the rations of ethylene glycol to water is 36:1,18:1,13:1). If only ethylene glycol was used as solvent, Ni/α-$Ni(OH)_2$ was obtained in form of irregular sheets and bulk material morphology (Figure S6a). It is found that the optimal solvents

ratio for the formation of uniform 2D mesoporous sheets of pure phase α-$Ni(OH)_2$ was 36:1(Figure S6b). And the increased ratio resulted in the increased thickness and disturbed uniformity of the sheets (Figure S 6c, 6d). If water was used individually, irregular sheets together with non-uniform nanoplates were produced (Figure S6e).

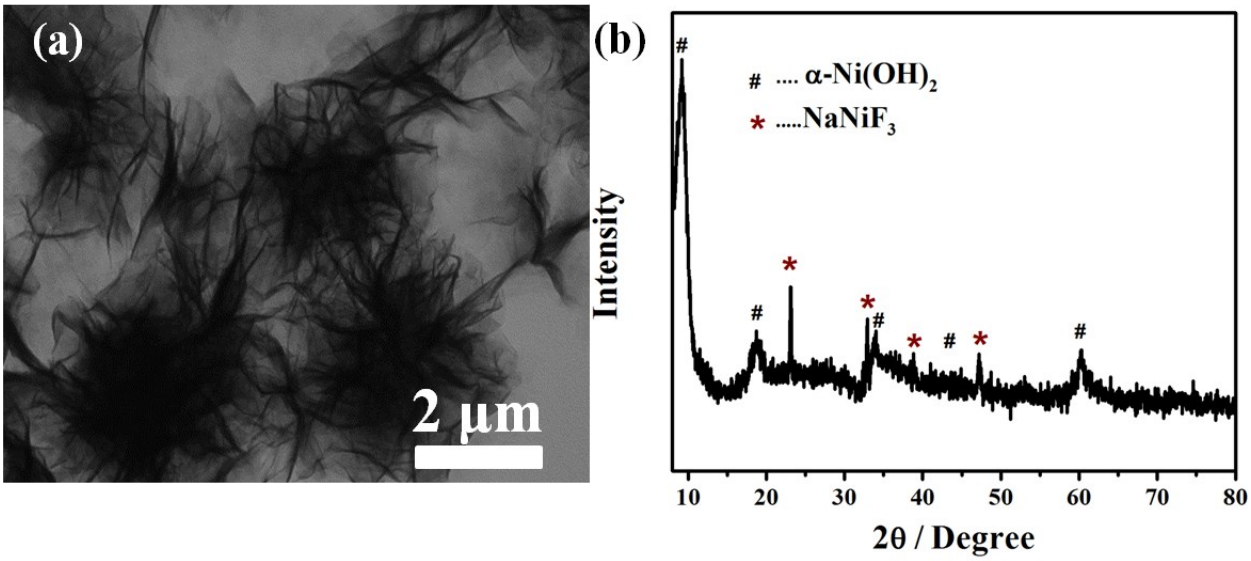

Figure S 5. (a) TEM image, (b) XRD pattern of prepared α-$Ni(OH)_2$ in the absence of sodium acetate.

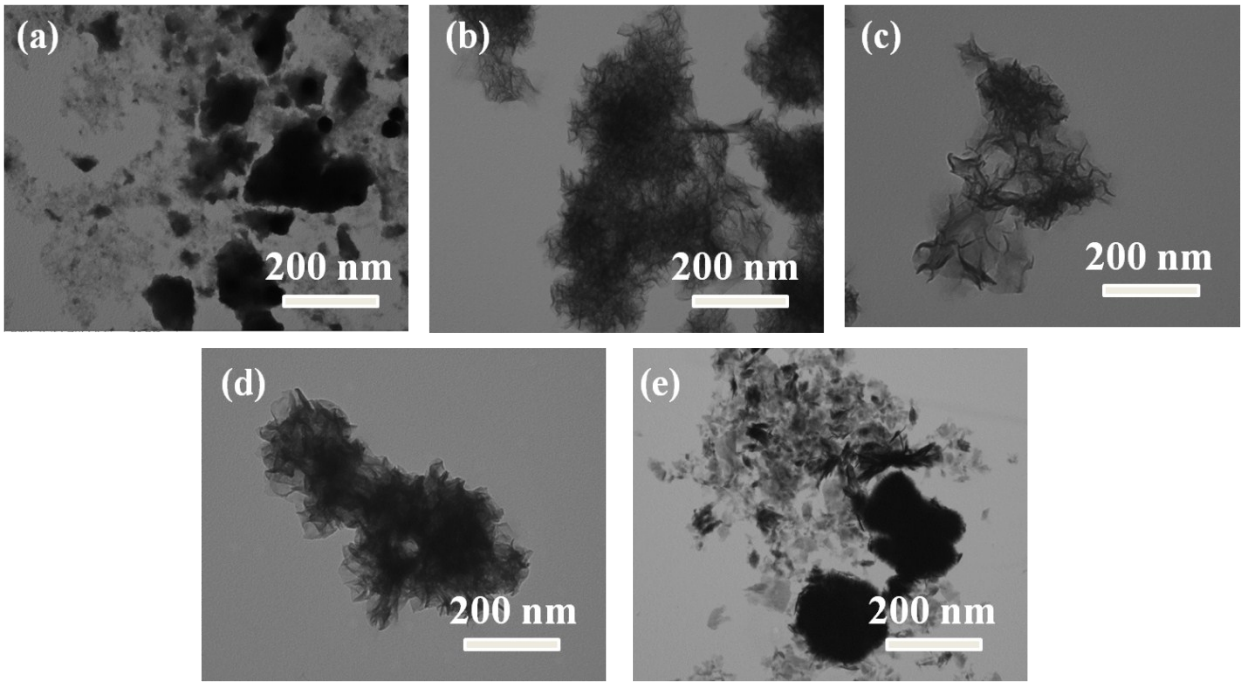

Figure S 6. TEM images of prepared samples at different concentrations of solvents: (a) only ethylene glycol, (b) 36:1 (EG: H_2O), (c) 18:1, (d) 13:1, (e) only water.

To investigate the growth processes of 2D mesoporous nanosheets, corresponding contrast experiments were performed at 200°C. It is found that no green solid was obtained when heating time was less than 30 minutes. Figure S7 shows the TEM images of green solids collected at different time. At beginning, nanosheets were formed along with bulk material (Figure S7a). As reaction progressed, bulk material continued transferred into 2D sheets (Figure S 7b, 7c and 7d). Uniform 2D curly mesoporous sheets of high yield were obtained when the reaction time was 12 h (Figure S7e). However, α-$Ni(OH)_2$ was partially decomposed (means Ni/α-$Ni(OH)_2$ Co-existed) if the reaction time was further extended to 15h (Figure S8). The above proportional experiments indicate that 12 h was optimal time to get pure phase F-doped α-$Ni(OH)_2$. From above results, following assumptions can be made: (1) pH of the reaction mixture effects on the formation of F-doped α-$Ni(OH)_2$. (2) Both temperature and reaction time are crucial for the formation of 2D porous sheets (3) Limited amount of water in ethylene glycol is helpful to generate pure phase of

F-doped α-$Ni(OH)_2$ with large d-spacing. Last but not least, NH_4F shows dual nature; First, it was crucial for the formation of α-$Ni(OH)_2$ nanostructure, Secondly, presence of F may increase the concentration of water between the layers which caused large d-spacing and better electrochemical performance.

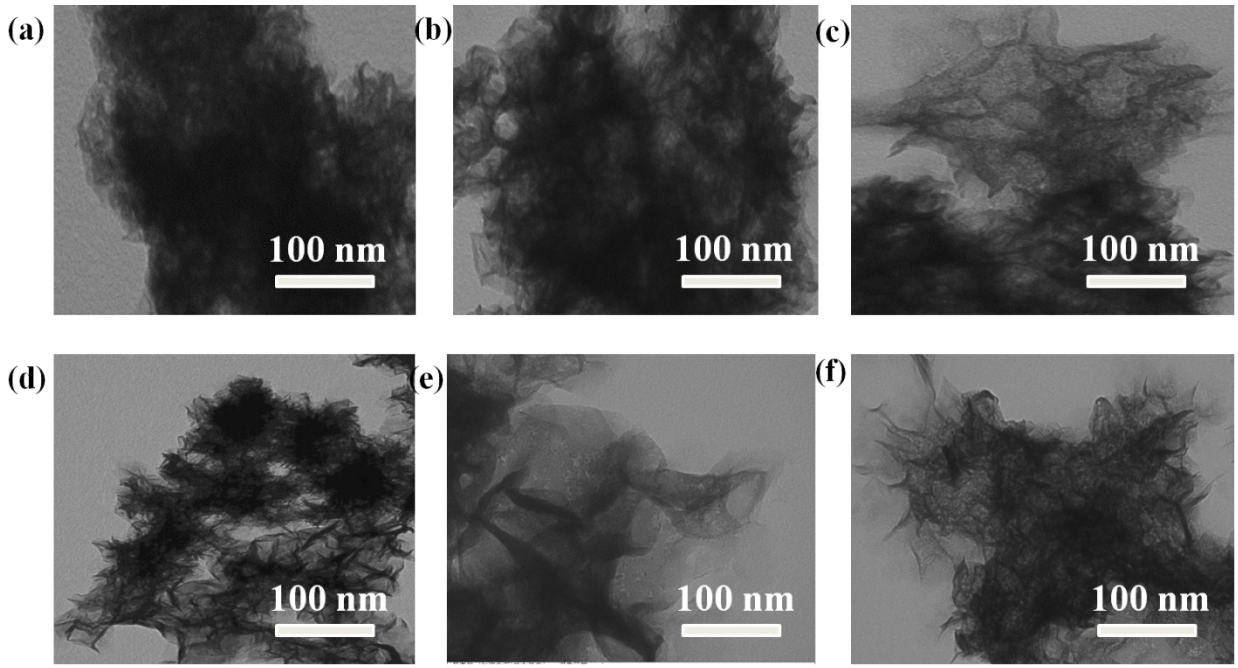

Figure S 7. TEM images of prepared samples at different heating time, (a) 1 h, (b) 3 h, (c) 6 h, (d) 9 h, (e) 12 h, (f) 15 h.

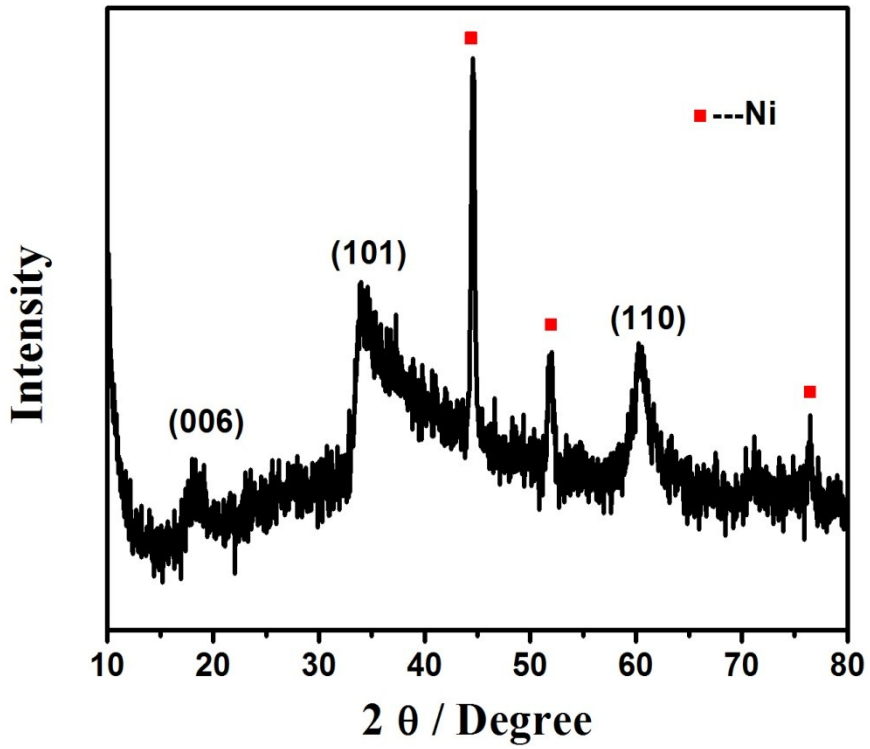

Figure S 8. XRD pattern of as prepared sample after heating of 15 h.

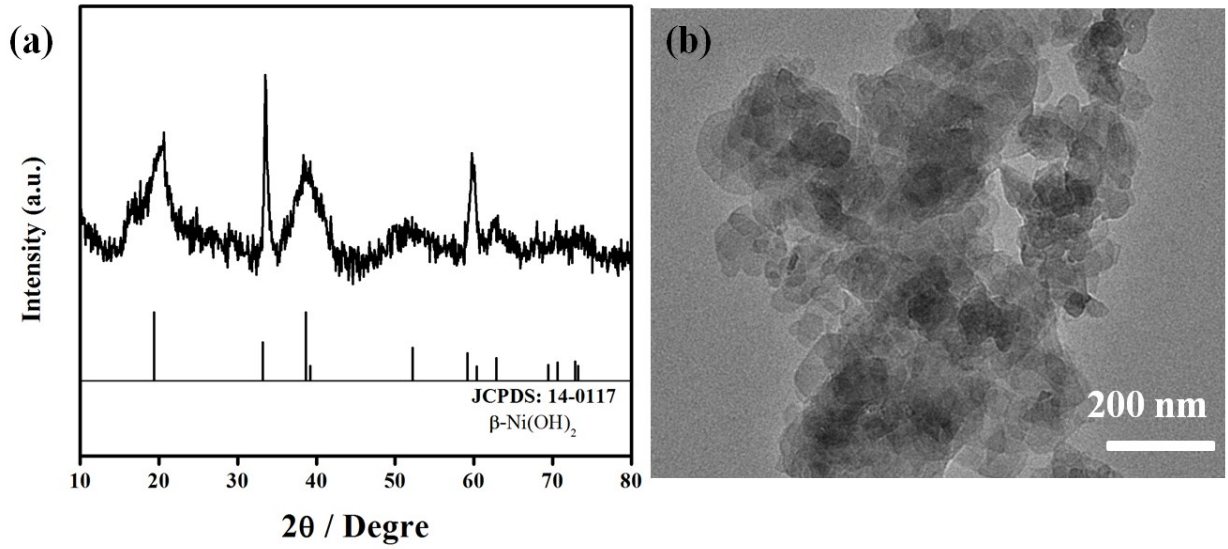

Figure S 9. Typical XRD pattern (a) and TEM image (b) of β-$Ni(OH)_2$.

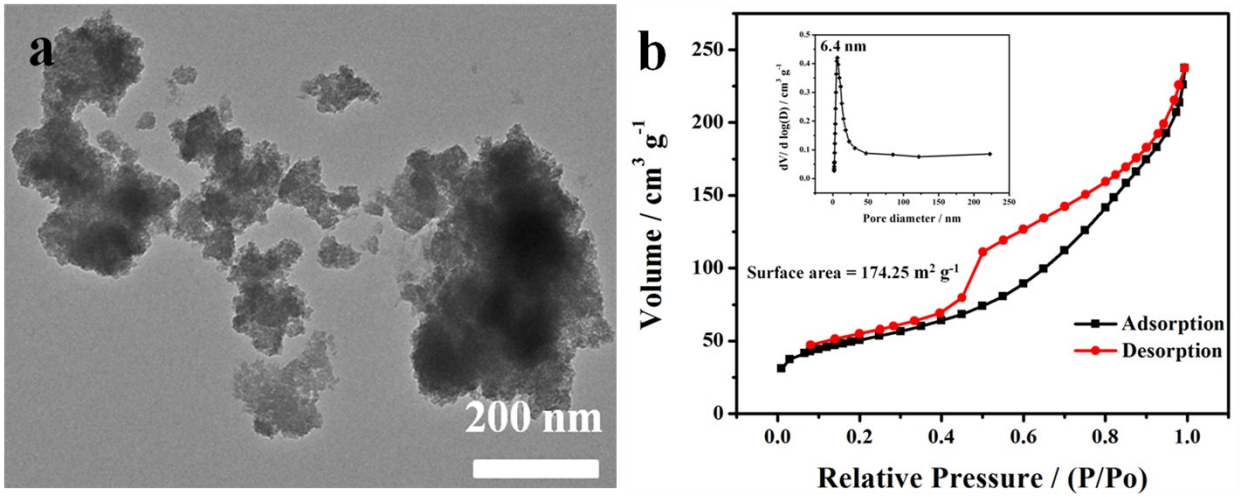

Figure S 10. A typical TEM image (a), Adsorption-desorption isotherm with pore size distribution (b) of α-$Ni(OH)_2$.

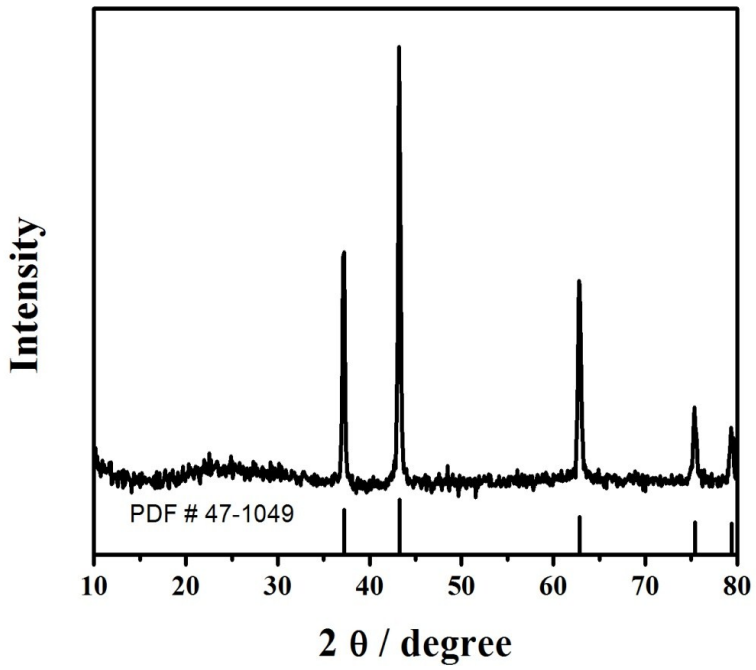

Figure S 11. A typical XRD pattern of the product obtained after TGA test of F-doped α-$Ni(OH)_2$.

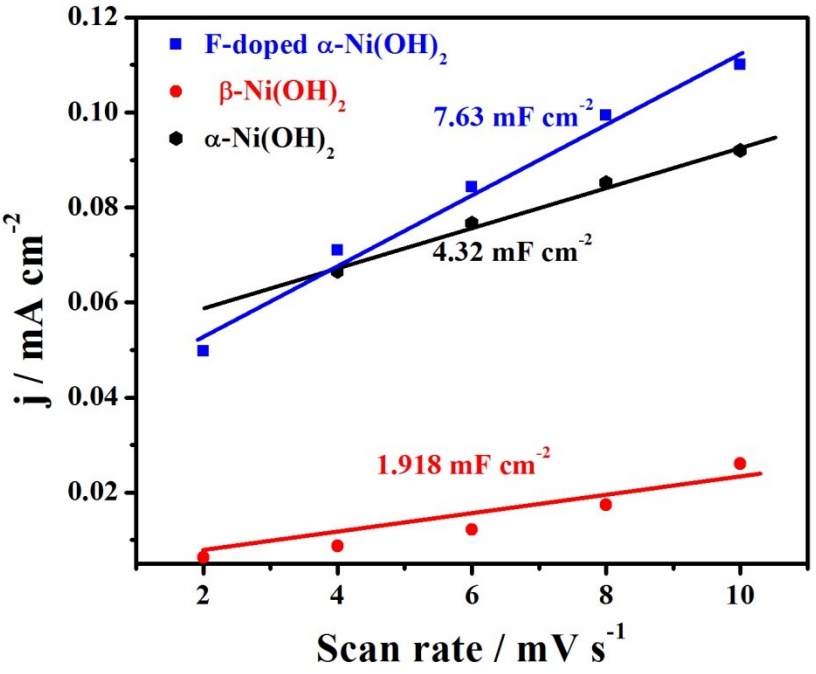

Figure S 12. Double layer capacitance measured at 1.18 V vs RHE from CV curves at different scan rates (2-10 mV s^{-1}) in the voltage window 1.12-1.22 vs RHE.

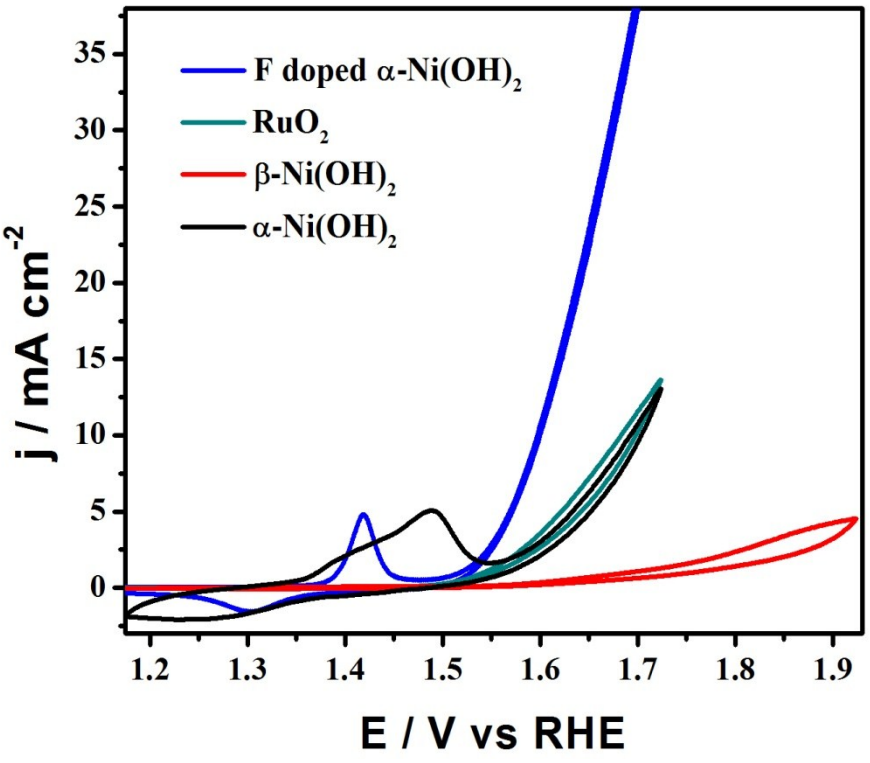

Figure S 13. 1st CV cycle of different studied catalysts.

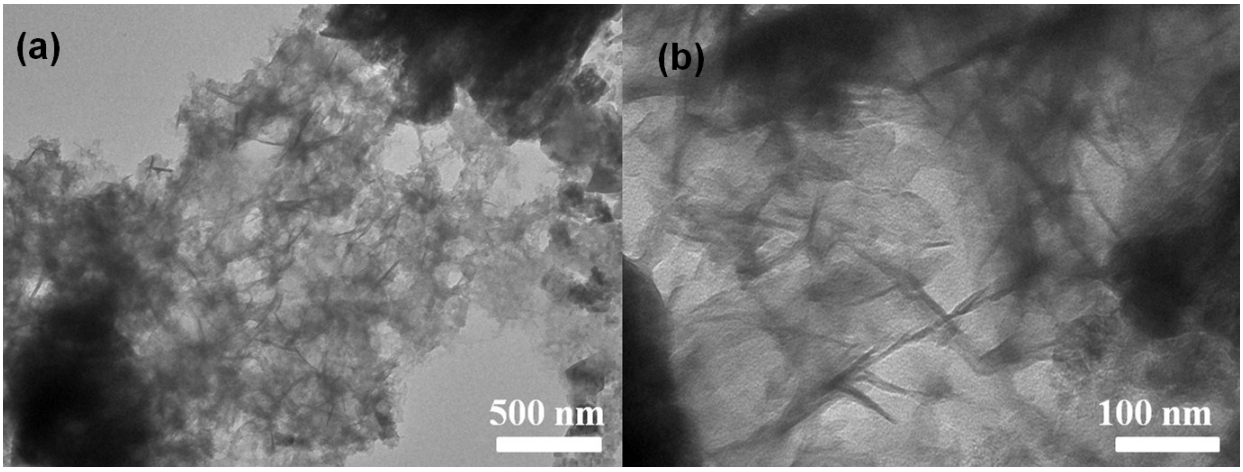

Figure S 14. TEM images of F-doped α-$Ni(OH)_2$ as a OER catalyst after stability test.

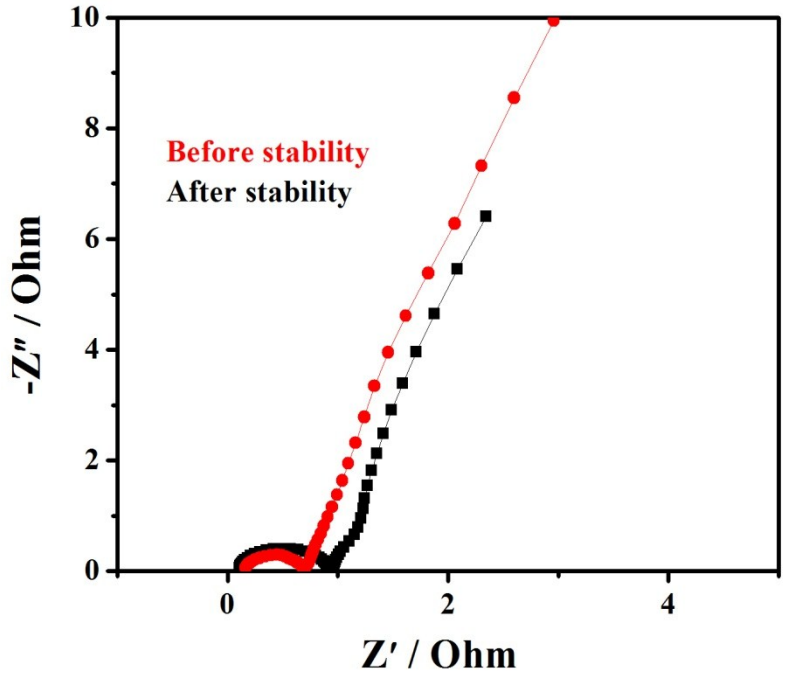

Figure S 15. Nequist plots at 300 mV before and after stability test.

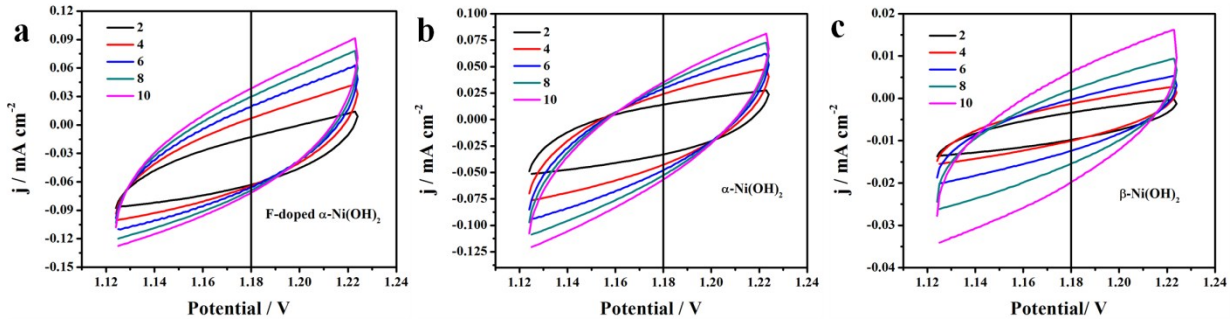

Figure S 16. CVs at different scan rates of in a potential window range from 1.12 to 1.22 V vs RHE for the (a) F-doped α-$Ni(OH)_2$, (b) α-$Ni(OH)_2$ and β-$Ni(OH)_2$.

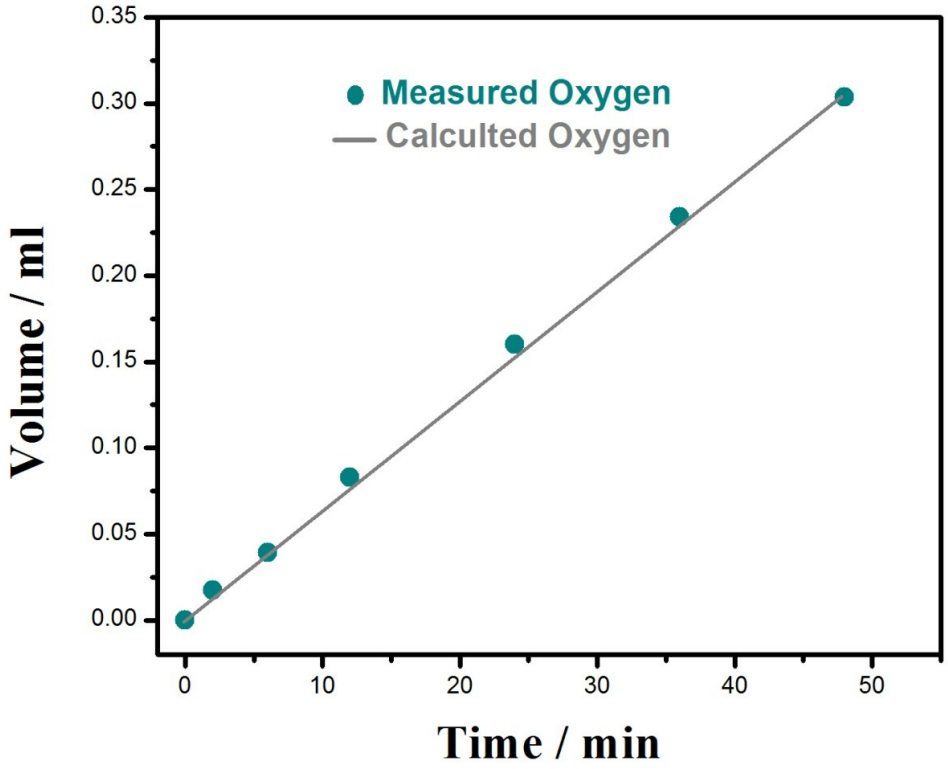

Figure S 17. Generated O_2 volume over time verses theoretical quantities assuming a 100 % Faradaic efficiency for the water splitting of F-doped α- $Ni(OH)_2$ in 1 M KOH at 1.7 V vs RHE.

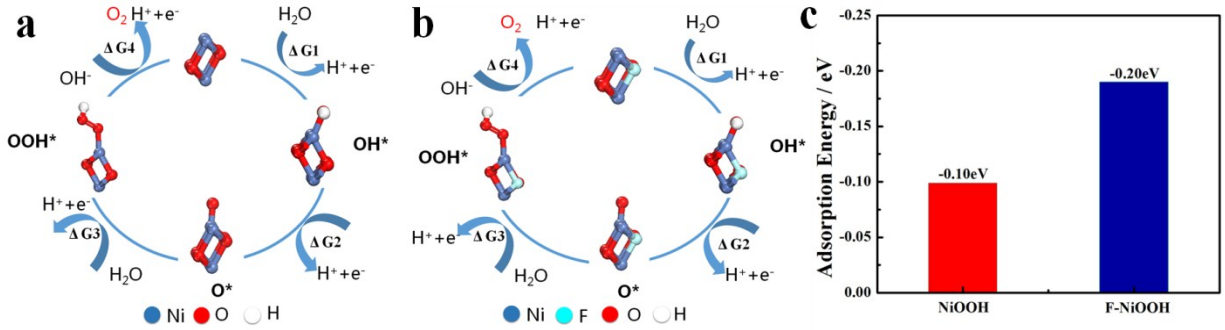

Figure S 18. (a) Primitive steps of the OER process of NiOOH. (b) Primitive steps of the OER process of F-NiOOH. (c) The adsorption energy of H2O on the NiOOH and F-NiOOH.

Tabel S1. Calculated Gibbs free energies (eV) of OER elementary steps under reaction condition (U = 0.88 V, pH = 14) on NiOOH(100) surface at the temperature of 298K.

	ΔE	ΔH	ΔZPE	TΔS	ΔG_U	ΔG_{pH}	ΔG
$H_2O(l)+*\rightarrow OH*+H^++e^-$	-0.88	-0.059	-0.085	-0.47	-0.32	0.84	-0.88
$OH*\rightarrow O*+H^++e^-$	4.18	0.044	-0.141	0.202	-0.32	0.84	3.56
$O*+ H_2O(l)\rightarrow OOH*+H^++e^-$	-0.88	-0.059	-0.151	-0.47	-0.32	0.84	-0.94
$OOH*\rightarrow * +O_2+H^++e^-$	2.82	0.044	-0.119	0.837	-0.32	0.84	1.58

Tabel S2. Calculated Gibbs free energies (eV) of OER elementary steps under reaction condition (U = 0.88 V, pH = 14) on F-NiOOH (100) surface at the temperature of 298K.

	ΔE	ΔH	ΔZPE	TΔS	ΔG_U	ΔG_{pH}	ΔG
$H_2O(l)+*\rightarrow OH*+H^++e^-$	-1.44	-0.059	-0.085	-0.47	-0.32	0.84	-1.43
$OH*\rightarrow O*+H^++e^-$	1.74	0.044	-0.141	0.202	-0.32	0.84	1.12
$O*+ H_2O(l)\rightarrow OOH*+H^++e^-$	2.65	-0.059	-0.151	-0.47	-0.32	0.84	2.58
$OOH*\rightarrow * +O_2+H^++e^-$	2.29	0.044	-0.119	0.837	-0.32	0.84	1.05

Table S3. Calculated frequencies, ZPE, and TΔS of OER elementary species under reaction condition (U = 0.88 V, pH = 14) at the temperature of 298K.

	Frequencies(cm-1)	ZPE(eV)	TΔS(eV)
$O_2(g)$	1558	0.1	0.62
$H_2(g)$	4408	0.27	0.42
$H_2O(g)$	1621, 3739, 3856	0.57	0.60

OH*	3545.97, 1280.15, 437, 17893, 161.29, 143.09	0.35	0
O*	825.90, 198.60, 183.89	0.074	0
OOH*	1736, 1326, 1188, 981, 196, 117, 90, 32, 20	0.358	0

Table S 4. Comparisons of OER activity data of present work with reported literature.

Catalyst	Mass loading (mg)	Electrolyte	η at j=10 mA cm^{-2} (mV)	Tafel slope at η=0.35 V ($mVdec^{-1}$)	Ref.
F-doped α- $Ni(OH)_2$	0.2	1 M KOH	325/GC 260/NF	31.89	This work
$Ni(OH)_2$ 2D-THNS	0.2	1 M KOH	335/GC	65	[13]
$Ni(OH)_2$ 2D-NS	0.2	1 M KOH	375/GC	81	[13]
CoNi(OH)x nanotubes		1 M KOH	280/Cu	77	[14]
Nickel Oxysulfide Hollow Nanospheres		1 M KOH	290/NF	62.38	[15]
$Ni(OH)_2$/NiAl foil		1 M KOH	289		[16]
CCS Ni-Co Nws	0.3	1 M KOH	302/CF	43.6	[17]
α- $Ni(OH)_2$	0.2	0.1 M KOH	331/GC	42	[18]
β- $Ni(OH)_2$	0.2	0.1 M KOH	444/GC	111	[18]
Ni_2Co_4	0.3	1 M KOH	>370/Ti	60	[19]
Ni–Co-Mixed Oxide		1 M NaOH	380/GC	50	[20]
$NaNiO_2$	0.13	1 M KOH	330/GC	60	[21]
NiD-PCC		1 M KOH	360	98	[22]
$LiNi_{0.8}Al_{0.2}O_2$	0.051	0.1 M KOH	350	44	[23]
NiV-LDH	0.143	1 M KOH	320	50	[24]
$Ni(OH)_2$ nanosheets (liquid phase exfoliation)	0.6	1 M NaOH	297/NF	60	[25]
RuO_2	0.25	0.1 M KOH	490		[26]

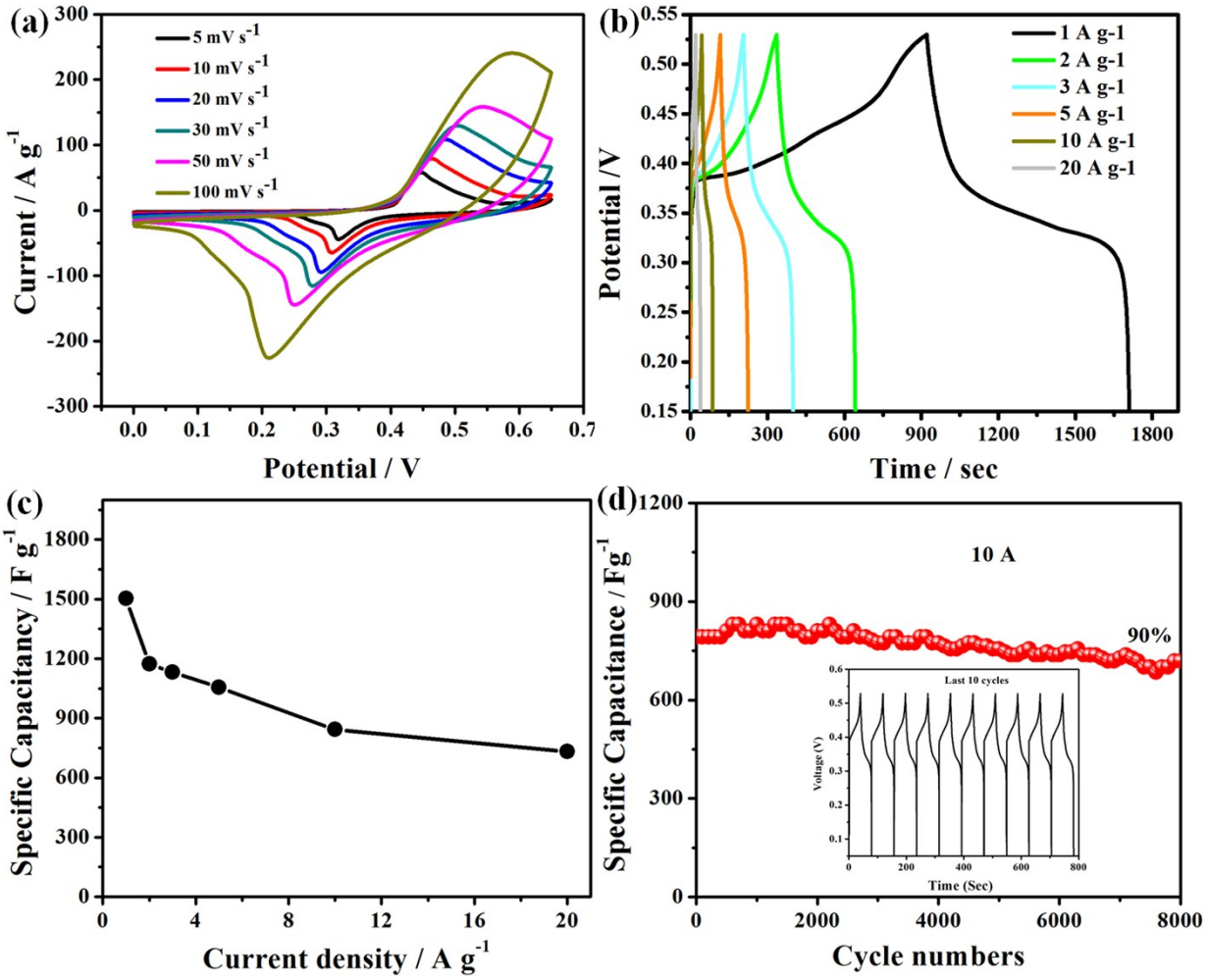

Figure S 19. Electrochemical performance of F-doped α-Ni(OH)$_2$ during three-electrode testing. (a) CV curves at different scan rates within voltage window 0-0.65 V. (b) Glavanostatic charging/discharging curves at different current densities as a function of scan rate. (c) Specific capacitance calculated at current densities within voltage window 0-0.53 V. (d) Cycling performance at current density of 10 A g^{-1} for 8000 cycles. The inset shows the final 10 charging/discharging cycles.

Figure S19a shows the CV curves at different scan rates (5-100mv) in the voltage window ranging from 0 to 0.65V. All the CV curves show pair of redox peaks, suggesting that the capacitance behavior based on faradic processes in which electrolyte adsorption takes place on the surface of electroactive material during reversible process. It is found that the positions of peaks

were slightly shifted owing to electrode polarization along with the increasing of the scan rate, but the shape of CV curves retained, indicating the good rate capacity. Figure S19b shows the galvanostatic charge-discharge (GCD) curves at current densities of 1, 2, 3, 5, 10 and 20 Ag^{-1} within voltage window of 0-0.53 V. The nonlinear charging and discharging curves suggesting the pseudocapacitive processes also confirm CV results. The specific capacitance at various current densities is shown in Figure S19c. F-doped α-$Ni(OH)_2$ exhibited a high specific capacitance 1503 F g^{-1} at current density 1 A g^{-1} and 732 F g^{-1} at current density 20 A g^{-1}, which was 63 % of the capacitance calculated at 2 A g^{-1}, indicating excellent rate capability of electrode. Cyclic stability was tested for further elaboration of long term sustainability and high performance of electrode (Figure S19d). F-doped α- $Ni(OH)_2$ retained 90% capacitance after 8000 cycles at a high current density of 10 A g^{-1}, which is much better than reported individually $Ni(OH)_2$ and $Ni(OH)_2$ based composite (Table S6). During the 1st to 500 cycles, the increase in capacitance was observed, which might be attributed to the activation period of $Ni(OH)_2$. The stable charge-discharge curves for the last ten cycles (inside in Figure S19d) further evidenced long term stability of F-doped α-$Ni(OH)_2$.

Table S5. Comparison of supercapacitor performance of present work with reported literature.

Sample	Electrolyte	Voltage Window (V)	Specific Capacitance (F g-1)	Cyclic Stability Retention	Ref.

F-doped α- $Ni(OH)_2$	2 M KOH	0-0.53	1503 at 1 A g^{-1}	90 % (8000 cycles)	This work
$FeOF/Ni(OH)_2$	3 M KOH	0-0.5	1452 at 1 A g^{-1}		[27]
Y-doped α-$Ni(OH)_2$	6 M KOH	0-0.4	1860 at 1 A g^{-1}	78 % (5000 cycles)	[28]
$Ni(OH)_2@Mn_2O_3$	6 M KOH	0-0.5	1219.1 at 2 A g^{-1}	90 % (1000 cycles)	[29]
$ZnO/Ni(OH)_2$	1 M NaOH	0-0.45	1830 at 2 A g^{-1}	80 % (1000 cycles)	[30]
β-$Ni(OH)_2$/Ni	2 M KOH	0-0.5	2384.3 at 1 A g-1	75 % (3000 cycles)	[31]
Amorphous nickel hydroxide	1 M KOH	0-0.5	2188 at 1mV sec^{-1}	76 % (10000 cycles)	[32]

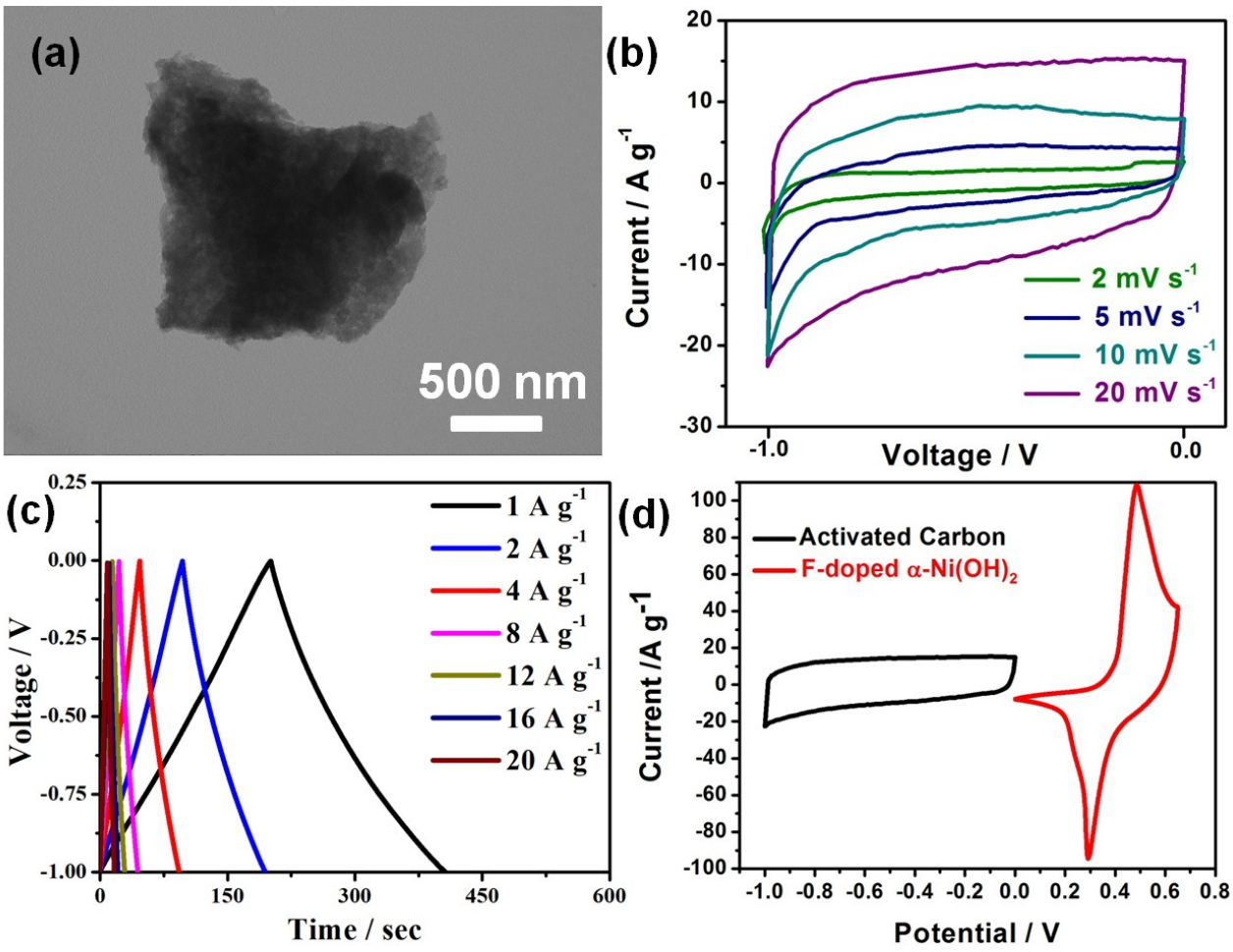

Figure S 20. (a) TEM image of activated carbon, (b) CV curves of AC at different scan rates (2-20 mV s^{-1}) within the voltage window from -1 to 0 V, (c) GCD curves of activated carbon at different current densities (d) CV curves of AC and F-doped α-$Ni(OH)_2$ at scan rate 20 mV s^{-1} in 2 M KOH.

References

1. C. C. McCrory, S. Jung, J. C. Peters and T. F. J. J. o. t. A. C. S. Jaramillo, *J. Am. Chem. Soc.*, 2013, **135**, 16977-16987.
2. J. P. Perdew, K. Burke and M. Ernzerhof, *Phy. Rev. Lett.*, 1996, **77**, 3865.
3. G. Kresse, *Comput. Mater. Sci.*, 1996, **6**, 15.
4. G. Kresse, *Phys. Rev. B*, 1996, **54**, 11169.
5. P. Blöchl, *Phys. Rev. B*, 1994, **50**, 17953.
6. W. H. Press, B. P. Flannery, S. A. Teukolsky and W. T. Vetterling, *Journal*, 1986.
7. J. K. Nørskov, J. Rossmeisl, A. Logadottir, L. Lindqvist, J. R. Kitchin, T. Bligaard and H. Jonsson, *J. Phy. Chem. B*, 2004, **108**, 17886-17892.
8. J. Rossmeisl, Z.-W. Qu, H. Zhu, G.-J. Kroes and J. K. Nørskov, *J. Electroana. Chem.*, 2007, **607**, 83-89.
9. J. T. Tables, D. Stull and H. Prophet, *US National Bureau of Standards, Washington, DC*, 1971.
10. E. C. Gonzalo, M. L. Sanjuán, M. Hoelzel, M. T. Azcondo, U. Amador, I. Sobrados, J. s. Sanz, F. García-Alvarado and A. Kuhn, *Inorganic Chemistry*, 2015, **54**, 3172-3182.
11. R. Pisarev, *SOVIET PHYSICS SOLID STATE, USSR*, 1965, **7**, 1114-+.
12. W. Rüdorbf, J. Kandler and D. Babel, *Zeitschrift für anorganische und allgemeine Chemie*, 1962, **317**, 261-287.
13. X. Kong, C. Zhang, S. Y. Hwang, Q. Chen and Z. Peng, *Small*, 2017, **13**, 1700334.
14. S. Li, Y. Wang, S. Peng, L. Zhang, A. M. Al-Enizi, H. Zhang, X. Sun and G. Zheng, *Adv. Energy Mater.*, 2016, **6**, 1501661.
15. J. Liu, Y. Yang, B. Ni, H. Li and X. Wang, *Small*, 2017, **13**, 1602637.
16. S. Niu, W. J. Jiang, T. Tang, Y. Zhang, J. H. Li and J. S. Hu, *Adv. Sci.*, 2017, **4**, 1700084.
17. S. H. Bae, J. E. Kim, H. Randriamahazaka, S. Y. Moon, J. Y. Park and I. K. Oh, *Adv. Energy Mater.*, 2017, **7**, 1601492.
18. M. Gao, W. Sheng, Z. Zhuang, Q. Fang, S. Gu, J. Jiang and Y. Yan, *J. Am. Chem. Soc.*, 2014, **136**, 7077-7084.
19. Z. Peng, D. Jia, A. M. Al-Enizi, A. A. Elzatahry and G. Zheng, *Adv. Energy Mater.*, 2015, **5**, 1402031.
20. L. Han, X. Y. Yu and X. W. Lou, *Adv. Mater.*, 2016, **28**, 4601-4605.
21. B. Weng, F. Xu, C. Wang, W. Meng, C. R. Grice and Y. Yan, *Energy Environ. Sci.*, 2017, **10**, 121-128.
22. M.-S. Balogun, W. Qiu, H. Yang, W. Fan, Y. Huang, P. Fang, G. Li, H. Ji and Y. Tong, *Energy Environ. Sci.*, 2016, **9**, 3411-3416.
23. A. Gupta, W. D. Chemelewski, C. Buddie Mullins and J. B. Goodenough, *Adv. Mater.*, 2015, **27**, 6063-6067.
24. K. Fan, H. Chen, Y. Ji, H. Huang, P. M. Claesson, Q. Daniel, B. Philippe, H. Rensmo, F. Li and Y. Luo, *Nat. Commun.*, 2016, **7**, 11981.
25. A. Harvey, X. He, I. J. Godwin, C. Backes, D. McAteer, N. C. Berner, N. McEvoy, A. Ferguson, A. Shmeliov and M. E. Lyons, *J. Mater. Chem. A*, 2016, **4**, 11046-11059.
26. S. Yagi, I. Yamada, H. Tsukasaki, A. Seno, M. Murakami, H. Fujii, H. Chen, N. Umezawa, H. Abe and N. Nishiyama, *Nat. Commun.*, 2015, **6**, 8249.
27. M. Wang, Z. Li, C. Wang, R. Zhao, C. Li, D. Guo, L. Zhang and L. Yin, *Adv. Funct. Mater.*, 2017, **27**, 1701014.
28. Y. Zhang, Y. Zhao, W. An, L. Xing, Y. Gao and J. Liu, *J. Mater. Chem. A*, 2017, **5**, 10039-10047.

29. Q. Ren, R. Wang, H. Wang, J. Key, D. J. Brett, S. Ji, S. Yin and P. K. Shen, *J. Mater. Chem. A*, 2016, **4**, 7591-7595.
30. I.-H. Lo, J.-Y. Wang, K.-Y. Huang, J.-H. Huang and W. P. Kang, *J. Power Sources*, 2016, **308**, 29-36.
31. X. Xiong, D. Ding, D. Chen, G. Waller, Y. Bu, Z. Wang and M. Liu, *Nano Energy*, 2015, **11**, 154-161.
32. H. Li, M. Yu, F. Wang, P. Liu, Y. Liang, J. Xiao, C. Wang, Y. Tong and G. Yang, *Nat. Commun.*, 2013, **4**, 1894.